SciEn

Proceedings of 8th International Conference on Mechanical Engineering and Renewable Energy 2025
10-12 December, 2025, Chattogram, BANGLADESH

SciEn Conference Series: Engineering Vol. 4, 2026, pp 555-560 https://doi.org/10.38032/scse.2026.4.240

Impacts of Hemodynamic Parameter on Two Different Sac Size Aneurysm Model at End Systolic and End Diastolic Velocity and Its Variation with Time-Averaged Velocity

Md. Parvez Mahmud[1,], Md Ajwad Mohimin[2], Sultan Hussain Labib[1] and Md. Mamunur Roshid[1]*

[1] Department of Mechanical Engineering, Chittagong University of Engineering and Technology, Chattogram, Raozan-4349, Bangladesh

[2]Department of Biomedical Engineering, Texas A&M University, College Station, TX-77840, USA

ABSTRACT

Hemodynamic parameters like Wall Shear Stress (WSS) and pressure are crucial to predict aneurysm behavior, including growth, stability, and rupture risk. And thus, they can assist the treatment decision. Our objective in this study is to observe variations in such parameters on two different aneurysm models having different sac sizes. This study will investigate End Systolic Velocity (ESV) and End Diastolic Velocity (EDV), and how they affect the hemodynamic parameters. It is expected that these two extreme conditions will provide a good overview of the aneurysm hemodynamics. In this work, the Time-Averaged (TA) inlet flow rate has also been introduced as a baseline reference to compare with the two extremes. ESV gives greater WSS and wall pressure than EDV on both models. This will impose more growth in the sac site in the small sac model. Differences in average WSS were observed between the two aneurysm geometries. The inclusion of TA allows quantification of the relative variations at diastolic and systolic conditions, demonstrating that ESV greatly amplifies WSS compared to TA, whereas EDV remains considerably lower.

Keywords: Hemodynamics, End Systolic Velocity, End Diastolic Velocity, Cerebral Aneurysm, Non-Newtonian Fluid.

1. Introduction

Aneurysm is a balloon-like structure commonly associated with the arteries. Although the exact reason for forming an aneurysm is not completely known, weakening of the wall may be a responsible factor [1]. Cerebral Aneurysm is one of a kind. Based on the angioarchitecture of cerebral aneurysms, fusiform and saccular aneurysms are generally observed. Among these two aneurysms, the saccular aneurysm is the most common one. A study of 329 cases revealed 95% of aneurysms were saccular [2].

Statistics say 2% of adult can have an aneurysm [3]. Among those, some may have the tendency to grow and eventually can rupture. Ruptured IA leads to bleeding in the brain and this phenomenon in medical study is called subarachnoid hemorrhage (SAH). Studies say almost 0.05% rupture occurs in a year from an unruptured intracranial aneurysm for size less than 10mm. This is a collected data from cumulative 7.5 years rupture rate for unruptured intracranial aneurysm (UIA) [4]. A 10-year cohort study by Zhong *et al.* [5] showed over 56 ruptured cases among 1960 aneurysms with a rate of 0.76%. The study also showed the high-risk factor with Hazard ratio (12.24) for aneurysm greater than 5mm. Women have generally higher risk of rupture than male which is surprisingly 1.4 times more after age of 55.

The study of Samar et al. says that around 78% of CFD studies assume blood as a Newtonian fluid [6]. The Carreau-Yasuda model predicted lower viscosity near the wall compared to Newtonian flow which can lead to overestimation of WSS and wrong assumptions for further procedures. That is why Newtonian flow assumption to capture the accurate rheology is not that much reliable [7]. Xiang *et al.* [8] studied four different typical saccular aneurysms with four different waveforms but with the same inflow rate as inlet boundary condition i.e. sixteen CFD simulations were performed in that study. The analysis revealed under the same mean inflow, different waveforms produced almost identical WSS and OSI distribution and similar maximum WSS.

The hemodynamic factors are also influenced by the aneurysm geometry, blood properties and flow conditions. In a study, five size and eight shape factors were introduced along with their impacts on hemodynamic factors [9]. Depending on size ratio (SR), there is a suggested cut-off value of 2.3 for predicting aneurysm rupture. Similarly, aspect ratio (AR) also has influence in aneurysm rupture which is considered in a broader range from 0.95 to 3.4 [10]. Moreover, blood properties, i.e., hematocrit is found to have influence over the hemodynamic parameters [11]. Although arterial blood flow is inherently pulsatile, it is convenient to use steady flow simulation to predict such factors avoiding higher computational cost. But there must be a proper selection of steady flow conditions which may be of time averaged (TA) velocity, ESV and EDV. Since for small intracranial aneurysm blood flow remains mostly laminar and the WSS and velocity distribution patterns are not significantly altered, TA flow field sufficiently represents the overall hemodynamic patterns. Geers *et al.* [12] showed in their study how the hemodynamic factors vary on these flow conditions but they took blood as Newtonian fluid. In this research our main objective is to find the variation under these steady flow conditions for blood taken as non-Newtonian fluid.

2. Physical Modeling and Meshing

2.1 Geometry description

Two patient-specific internal cerebral artery models described in Table 1 were chosen for this current study. The geometry was imported into Ansys Spaceclaim for further modification of the surface geometry through surface cleaning and smoothing, capping of open boundaries, and creating a fluid domain. Fig. 1 shows the model's geometry.

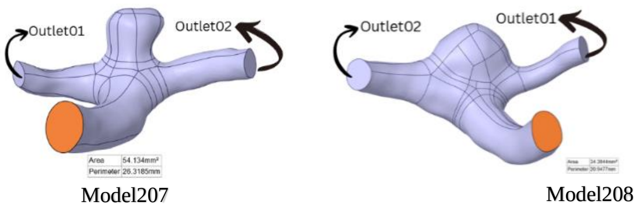

Fig. 1 Two models with parent artery flow area.

Table 1 Descriptions of two models.

Model ID	Aneurysm Location	Sex	Age (years)	Disease
207_H_CERE_CA	Left ICA	Female	61	Cerebral Aneurysm
208_H_CERE_CA	ICA	Female	71	Cerebral Aneurysm

2.2 Meshing

Body sizing of 1mm and inflation of smooth transition with 5 layers was imposed on the geometry. Proper name selection for boundary conditions was taken as inlet, outlet, artery wall, and fluid domain. Meshing is shown in fig. 2.

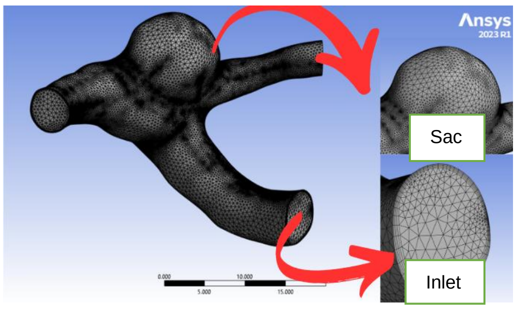

Fig. 2 Meshing of geometry.

3. Methodology and Numerical Analysis

3.1 Problem Description

Those two models, identical in both size and location, were taken from a case study of Allyson *et al.* [13]. Hemodynamics parameters like WSS, Wall pressure, were observed under three inlet boundary conditions: End Systolic Velocity (ESV), End Diastolic Velocity (EDV), and Time-Averaged velocity (TAV). Two extreme velocities were taken from literature [14] for the internal carotid arteries. In both models, values of ESV and EDV are 57cm/s and 18cm/s. Since the exact location of model208 wasn't mentioned as right or left ICA, the average value was taken.

3.2 Boundary Conditions

A uniform mass flow rate was imposed on the parent artery in the inlet section. Pressure-outlet condition was given in both outlets with an operating pressure of 13332 Pa. The artery wall was assumed to be rigid with no slip boundary condition, which is a limitation of this study.

3.3 Governing Equations

This study of fluid flow is governed by the continuity equation and the Navier-Stokes equation. For the incompressible and isothermal case, these equations can be written as follows:

$$\nabla \cdot u = 0 \tag{1}$$

$$\rho(\partial t/\partial u + u\cdot\nabla u) = -\nabla p + \mu\nabla 2u + f \tag{2}$$

The empirical relation of inlet blood flow rate given by Cebral *et al.* [15] is as follows:

$$Q_A = 48.21A^{1.84} \tag{3}$$

where Q_A is in ml/s and A is the inlet's cross-sectional area in cm^2.

The blood flow was considered to be laminar as a study on turbulence modeling showed minimal difference in the hemodynamic parameters [16]. Blood was modeled as an incompressible, shear-thinning, non-Newtonian fluid using the Carreau–Yasuda viscosity model, which captures the variation of dynamic viscosity with shear rate. The model is expressed as:

$$\mu(\dot{\gamma}) = \mu_\infty + (\mu_0 - \mu_\infty)\,[1 + (\lambda\dot{\gamma})^a]^{(n-1)/a} \tag{4}$$

Table 2 shows the model parameters for Eq. (4) as compiled by Young et al. [17]

Table 2 Model Parameters for Bird-Carreau non-Newtonian viscosity model.

Parameter	Symbol	Value	Unit
Zero-shear viscosity	μ_0	0.056	Pa·s
Infinite-shear viscosity	μ_∞	0.00345	Pa·s
Time constant	λ	3.313	s
Power-law index	n	0.3568	—

3.4 Mesh Independence Test

The mesh independence test is shown in fig. 3. Since the solution has been converged in between 1M element size, we took it as a threshold value. The convergence test was performed only in model208 under EDV boundary condition.

3.5 Data Evaluation

Wall shear stress is a key parameter in the context of aneurysmal hemodynamics. It is the tensile force exerted by the blood on the surface of the arterial wall. WSS can be responsible for initiation, growth and rupture of an IA [1]. The diastolic wall shear stress (DWSS) and systolic wall shear stress (SWSS) were calculated as the WSS averaged over the aneurysm surface at the diastolic minimum and systolic peak shown in Eq. (5) & (6).

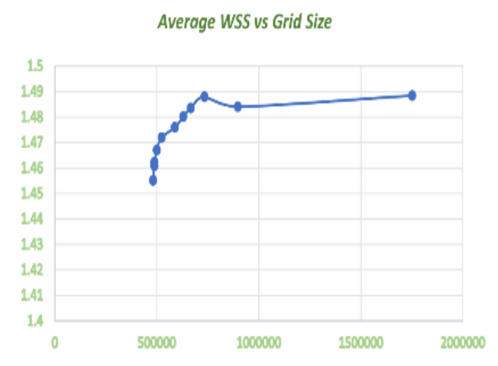

Fig. 3 Grid independence test.

$$SWSS = \frac{1}{A} \int_A \tau_w(x; U_s)\, dA \quad (5)$$

$$DWSS = \frac{1}{A} \int_A \tau_w(x; U_d)\, dA \quad (6)$$

The time-averaged WSS is calculated through the given equation:

$$TAWSS = \frac{1}{T} \int_0^T |\tau w(t)| dt \quad (7)$$

3.6 Model Validation

Fig. 4 shows the deviation of maximum time-averaged wall shear stress (TAWSS) of model207 compared with the numerical data evaluated from the case study from which the geometry was taken. Another deviation of model208 is also shown compared with a study [18] with almost similar boundary conditions.

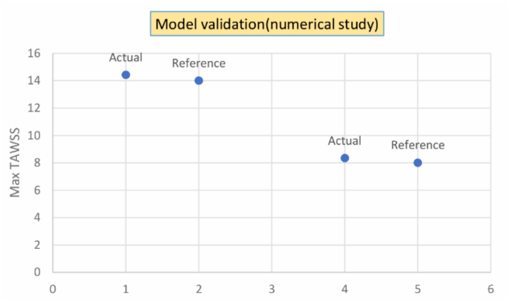

Fig. 4 Model validation with similar numerical study.

4. Results and Discussion

The influence of geometry and boundary conditions on the desired hemodynamic factors are analyzed in this section. Since inlet area of model207 is larger than model208 and the inlet boundary conditions are constant, model208 experiences more wall pressure and shear at the inlet. Outlet02 is located at the right side of model207 and at the left side of model208 as pictured in fig. 1. In the arterial bifurcation, the geometric alignment of the parent artery relative to the daughter branches strongly influences the flow distribution. Here, in both models the parent artery was more aligned to outlet02.

The inlet and outlet flow parameters are evaluated in Table 3 for all three-inlet steady flow boundary conditions. Mass flow rate for both models to be applied as inlet boundary condition was calculated from the inlet area and velocity. Due to parent artery alignment, as mentioned earlier, the velocity at outlet02 was higher than outlet01 for both models under each inlet boundary condition. Again, model207 persisted more velocity at each outlet under each boundary condition than model208. Though, for EDV and TA velocity condition, model208 persisted almost similar velocity at both outlets.

Fig. 5 represents the mass flow vs maximum pressure drop between the inlet and the outlet. Since the outlet velocity is maximum in outlet02 in comparison with the two outlets for both models, the maximum pressure drop occurred in outlet02 for each model calculated from the inlet.

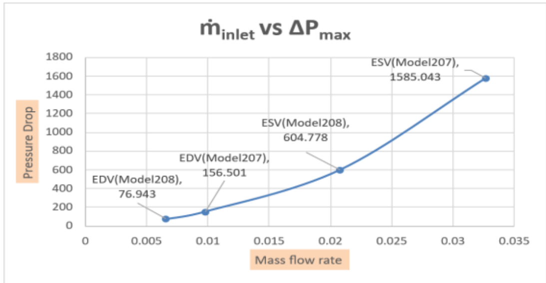

Fig. 5 Inlet Mass Flow vs Max Pressure drop between inlet and outlet.

The ESV condition of model207 introduced maximum mass flow rate, which provides maximum pressure drop than any other boundary condition. Here, in the graph, the pressure drop has increased with the increased mass flow. In model207, the pressure drop has increased more under ESV than EDV condition.

Fig. 6 shows the WSS distribution for both models. In model207, ESV and TA velocity conditions exhibit similar spatial distributions along the arterial wall, while differing primarily in magnitude. Similar distribution is also seen in model208 but for EDV and TA velocity. The neck region of model207 under ESV experiences the highest hemodynamic loading, making it the most affected and vulnerable region prone to expansion. In that case, the region vicinity to the dome in model208 is highly affected which may lead to more expansion. The WSS in the dome circumference of model208 shows minimal variation, whereas pronounced WSS fluctuations are observed in the dome of model207.

Fig. 7 shows the velocity distribution to observe the flow of blood. In model208, for EDV and TA velocity inlet boundary conditions, there is seen to be very low velocity near the wall, which is also responsible for low WSS (fig. 6). This may explain the effect of low WSS on an aneurysmal wall, as the mural cell proliferation can synthesize new collagen matrices, which may lead to wall expansion. Thus, this hemodynamic environment indicates that the model208 is highly prone to rupture due to sustained low near-wall velocity and chronically low WSS. Moreover, the inflow is much higher in the large dome model, and the model with the narrow neck experiences less inflow.

Table 3 Inlet and outlet blood flow parameters with static wall pressure.

Flow Condition	**Inlet Area (m^2)**	**Inlet Velocity (m/s)**	**Inlet Mass Flow (kg/s)**	**Outlet 01 Velocity (m/s)**	**Outlet 02 Velocity (m/s)**	**Wall Pressure (Pa)**
ESV (Model 207)	54.134	0.5714	0.0327	1.0101	1.1109	980.0965
ESV (Model 208)	34.394	0.5722	0.0208	0.4094	0.6210	296.4638
EDV (Model 207)	54.134	0.1704	0.00975	0.3053	0.3149	98.6327
EDV (Model 208)	34.394	0.1815	0.0066	0.1176	0.1970	37.7766
TAV(Model207)	54.134	0.2883	0.0165	0.5143	0.5488	248.4702
TAV(Model208)	34.394	0.1981	0.0072	0.1291	0.2155	43.7012

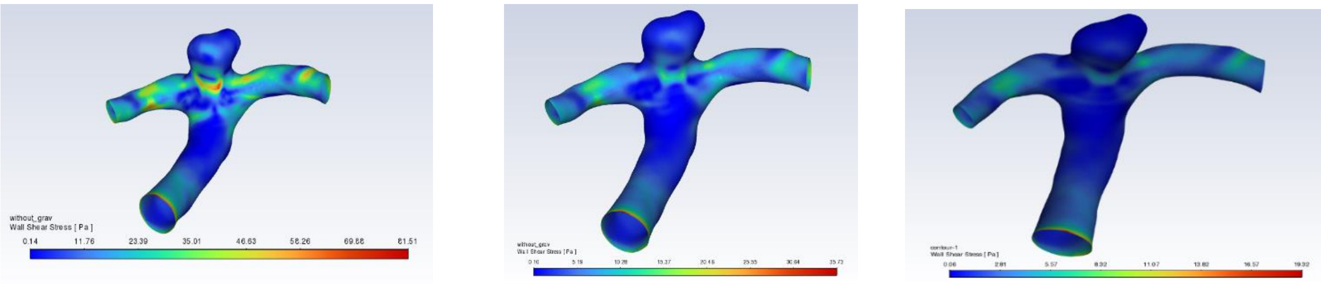

(a)

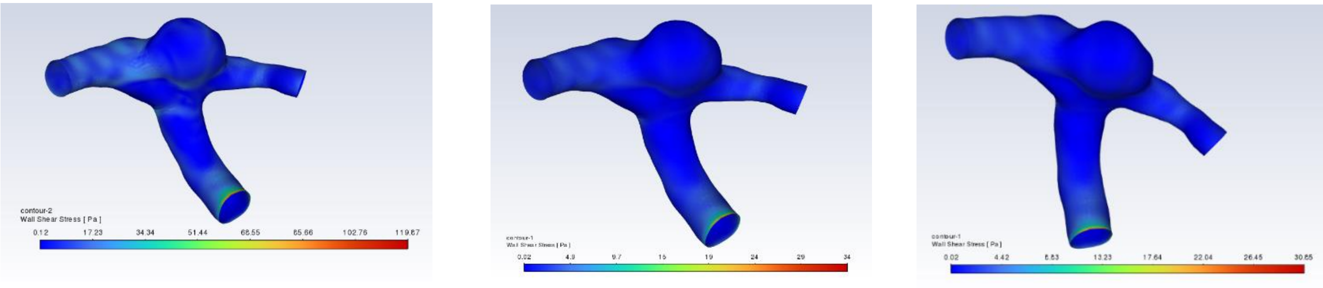

(b)

Fig. 6 WSS distribution on three inlet steady flow boundary conditions of ESV, EDV, and TA velocity for (a) Model207 and (b) Model208.

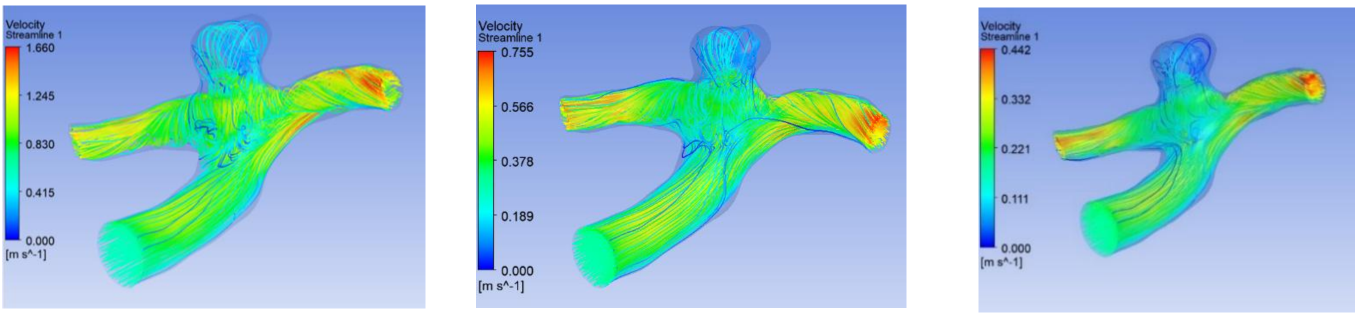

(a)

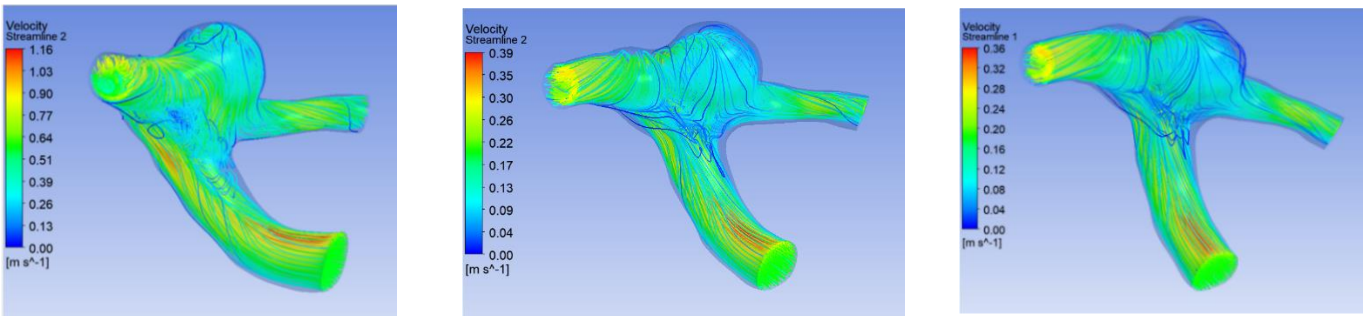

(b)

Fig. 7 Velocity distribution on three inlet steady flow boundary conditions of ESV, EDV and TA velocity for (a) Model207 and (b) Model208.

The time-averaged flow rate driven from the empirical equation is not certain; it may have some variation. The variation can be ±27%, which is the average relative error between prediction and measurement [15]. In this work, we will neglect the variation and take the TA flow rate as the baseline value. Taking the value as baseline, the WSS during diastole was approximately 13% lower than TA, while systolic flow elevated WSS by nearly 397% from TA in model208 shown in fig. 8. Here, it is also observed that EDV and TA velocity condition of model208 persist coherent relation in average WSS like the other parameters shown in Table 3.

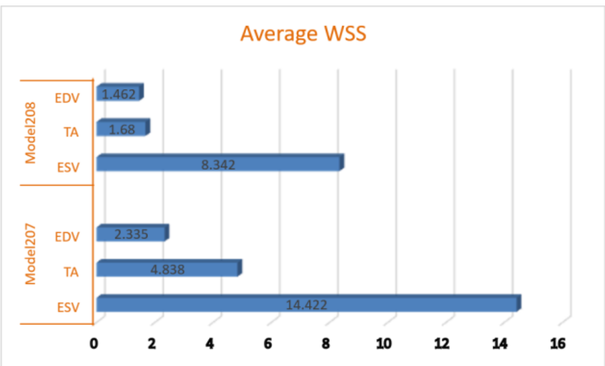

Fig. 8 Average Wall Shear Stress on ESV, TAV and EDV in two model.

In model207, the diastolic flow reduced average WSS by more than 52% compared to TA, whereas systolic inflow increased WSS by nearly 198%. For Model208, the average WSS at EDV and TA remained relatively low, with values of 1.462 Pa and 1.68 Pa, respectively. However, a strong increase was observed under ESV, where the average WSS reached 8.342 Pa, nearly five times higher than the TA value. This demonstrates the sensitivity of WSS to peak systolic conditions, highlighting that aneurysmal walls experience markedly higher hemodynamic loading during systole compared to the mean or diastolic phases. But, the EDV condition also has adverse effect on aneurysmal wall (fig. 6). Though, model207 is more affected by systolic condition than model208. The ESV condition exhibited the highest average WSS of 14.422 Pa, approximately three times larger than the TA and over six times greater than the EDV value. So, if timely and appropriate intervention is not undertaken, this elevated systolic loading may drive progressive wall remodeling, potentially leading to a transition from the hemodynamic state of model207 toward the more rupture-prone condition observed in model208.

5. Conclusion

This study investigated the hemodynamic environment of two aneurysm models with different sac sizes under ESV, EDV, and TA inlet conditions. Hemodynamic factors like WSS, wall pressure along with blood flow velocity, pressure drop was investigated simultaneously for each boundary condition. Overall, the study shows that areas exposed to low WSS and near-wall flow, especially in the wall regions of model208, are more likely to undergo wall weakening and expansion which increases the risk of rupture. In contrast, model207 is mainly affected by high systolic loading, where the neck region experiences the highest stress and is therefore the most vulnerable area for future expansion. The TA inlet condition evidently represented the mean hemodynamic loading experienced by the aneurysm wall of model207 rather than model208 and therefore can be used as a baseline reference for model like this. However, TA flow is widely adopted in computational hemodynamics as a practical surrogate for pulsatile inflow. Though the TA velocity taken from the empirical equation may deviate (±27%) from the true cycle-averaged waveform. In future work, this deviation can be taken into consideration. Future work can also incorporate transient and fluid structural analysis (FSI) with pulsatile velocity waveform to visualize more realistic aneurysm growth.

6. References

[1] N. Chalouhi, B. L. Hoh, and D. Hasan, "Review of cerebral aneurysm formation, growth, and rupture," Dec. 2013.

[2] M. B. Pritz, "Cerebral aneurysm classification based on angioarchitecture," *Journal of Stroke and Cerebrovascular Diseases*, vol. 20, no. 2, pp. 162–167, Mar. 2011,

[3] G. J. E. Rinkel, M. Djibuti, A. Algra, and ; J Van Gijn, "Prevalence and Risk of Rupture of Intracranial Aneurysms A Systematic Review," 1998. [Online]. Available: http://ahajournals.org

[4] R. Hurford, I. Taveira, W. Kuker, and P. M. Rothwell, "Prevalence, predictors and prognosis of incidental intracranial aneurysms in patients with suspected TIA and minor stroke: A population-based study and systematic review," May 01, 2021, *BMJ Publishing Group*. doi: 10.1136/jnnp-2020-324418.

[5] Y. Murayama *et al.*, "Risk Analysis of Unruptured Intracranial Aneurysms: Prospective 10-Year Cohort Study," *Stroke*, vol. 47, no. 2, pp. 365–371, Feb. 2016, doi: 10.1161/STROKEAHA.115.010698.

[6] S. A. Mahrous, N. Azwadi, C. Sidik, and K. M. Saqr, "CFD Letters Newtonian and non-Newtonian CFD Models of Intracranial Aneurysm: A Review," *CFD Letters*, vol. 12, pp. 62–86, 2020.

[7] J. Bernsdorf and D. Wang, "Non-Newtonian blood flow simulation in cerebral aneurysms," *Computers and Mathematics with Applications*, vol. 58, no. 5, pp. 1024–1029, Sep. 2009, doi: 10.1016/j.camwa.2009.02.019.

[8] J. Xiang, A. H. Siddiqui, and H. Meng, "The effect of inlet waveforms on computational hemodynamics of patient-specific intracranial aneurysms," *J. Biomech.*, vol. 47, no. 16, pp. 3882–3890, Dec. 2014, doi: 10.1016/j.jbiomech.2014.09.034.

[9] M. L. Raghavan, B. Ma, and R. E. Harbaugh, "Quantified aneurysm shape and rupture risk," 2005.

[10] C. W. Ryu, O. K. Kwon, J. S. Koh, and E. J. Kim, "Analysis of aneurysm rupture in relation to the geometric indices: Aspect ratio, volume, and volume-to-neck ratio," *Neuroradiology*, vol. 53, no. 11, pp. 883–889, Nov. 2011, doi: 10.1007/s00234-010-0804-4.

[11] M. A. Mohimin, N. M. Arefin, and P. Das, "Cerebral Aneurysm Hemodynamics in Low Hematocrit Conditions: Numerical Simulations and Analysis." [Online]. Available: https://ssrn.com/abstract=4889257

[12] A. J. Geers, I. Larrabide, H. G. Morales, and A. F. Frangi, "Approximating hemodynamics of cerebral aneurysms with steady flow simulations," *J. Biomech.*, vol. 47, no. 1, pp. 178–185, Jan. 2014, doi: 10.1016/j.jbiomech.2013.09.033.

[13] A. J. Weiss *et al.*, "A matched-pair case control study identifying hemodynamic predictors of cerebral aneurysm growth using computational fluid dynamics," *Front. Physiol.*, vol. 14, 2023, doi: 10.3389/fphys.2023.1300754.

[14] J. H. Chowdhury and K. K. Saha, "Measurement of Peak Systolic Velocities and End Diastolic Velocities of Common Carotid, Internal Carotid and Vertebral Arteries of Healthy Adult Subjects by Duplex Colour Doppler Sonography : A Study of 100 Cases," 2021.

[15] J. R. Cebral, M. A. Castro, C. M. Putman, and N. Alperin, "Flow-area relationship in internal carotid and vertebral arteries," *Physiol. Meas.*, vol. 29, no. 5, pp. 585–594, May 2008, doi: 10.1088/0967-3334/29/5/005.

[16] P. D. Md. A. I. H. S. Md. Ajwad Mohimin, "EFFECT OF RANS TURBULENCE MODEL ON THE HEMODYNAMIC FACTORS IN A MIDDLE CEREBRAL ARTERY ANEURYSM ," Chattogram: 7th International Conference on Mechanical Engineering and Renewable Energy 2023 , 2023.

[17] "Effects of the non-Newtonian viscosity of blood on hemodynamics of diseased".

[18] G. Carty, S. Chatpun, and D. M. Espino, "Modeling Blood Flow Through Intracranial Aneurysms: A Comparison of Newtonian and Non-Newtonian Viscosity," *J. Med. Biol. Eng.*, vol. 36, no. 3, pp. 396–409, Jun. 2016, doi: 10.1007/s40846-016-0142-z.

7. Nomenclature

Symbol	Meaning	Unit
∇	Nabla operator	Dimensionless
u	Velocity vector	m/s
ρ	Fluid density	kg/m^3
t	Time	s
P	Pressure	Pa
μ	Dynamic viscosity	Pa·s
f	Body force per unit volume	N/m^3
Q_A	Flow rate relation coefficient	m^3/s
A	Cross-sectional area	m^2
T	Duration of one cardiac cycle	s
U_s	Inlet velocity at systole	m/s
U_d	Inlet velocity at diastole	m/s
τ_w	Wall Shear Stress (WSS)	Pa